Journal of
Mechanics of
Materials and Structures

EXPANSION-CONTRACTION BEHAVIOR OF A PRESSURIZED POROHYPERELASTIC SPHERICAL SHELL DUE TO FLUID REDISTRIBUTION IN THE STRUCTURE WALL

Vahid Zamani and Thomas J. Pence

Volume 15, No. 1 January 2020

msp

JOURNAL OF MECHANICS OF MATERIALS AND STRUCTURES
Vol. 15, No. 1, 2020
dx.doi.org/10.2140/jomms.2020.15.159

msp

EXPANSION-CONTRACTION BEHAVIOR OF A PRESSURIZED POROHYPERELASTIC SPHERICAL SHELL DUE TO FLUID REDISTRIBUTION IN THE STRUCTURE WALL

VAHID ZAMANI AND THOMAS J. PENCE

Spherical shells with porohyperelastic walls that contain mobile liquid are examined for the purpose of determining how the in-wall liquid distribution affects the overall mechanical response. Attention is restricted to spherical symmetry and to Mooney–Rivlin type material models that are generalized so as to incorporate swelling. In this setting, different distributions of the same amount of liquid are examined for their effect on the sphere's pressure-expansion behavior. Liquid distributions that are essentially uniform are found to give the most compliant response. In contrast, nonuniform liquid distributions that concentrate liquid near either the inner or outer wall are found to stiffen the overall behavior. Liquid redistribution can also alter the basic monotonicity properties of the resulting inflation graphs, possibly leading to various limited burst events.

1. Introduction

Liquid infused soft solids, ranging from gels to biological tissue, exhibit complex mechanical and physical behavior as the liquid content varies. The underlying chemical and microstructural phenomena can be modeled at the continuum mechanics level [Drozdov 2013; Drozdov et al. 2018], and such modeling aids the development of soft material actuators [Stuart et al. 2010; Liu et al. 2018]. The focus of the present work is on how the specific liquid distribution influences the amount of deformation in a soft solid system that responds to mechanical load. In particular, we examine how a soft solid structure or mechanism with a *fixed liquid content* can undergo significant deformation simply by having the fixed amount of liquid redistributed in a different fashion within the system.

For this purpose we consider an internally pressurized spherical cell with "gel-type" cell walls, namely the walls consist of a liquid infused porohyperelastic material. This corresponds to a spherical balloon or bladder with liquid infused walls. The overall amount of liquid is fixed, but may redistribute itself within the bladder wall. Attention is restricted to spherically symmetric liquid distributions in order to permit a treatment that exploits spherical symmetry. At issue is how the liquid distribution affects the amount of overall expansion that is due to an internal pressurization.

We follow a continuum mechanical treatment that tracks change in the local liquid content in terms of the associated material volume change. Both the base soft porous ground substance and the mobile liquid constituent are regarded as incompressible. This causes the local amount of swelling v to be a proxy for the amount of mobile liquid that is currently resident. Prior to any settled equilibrium — meaning that there is still active liquid migration through the porous material — the description of the liquid seepage requires the consideration of the driving action of pore pressure gradients, osmotic pressure,

Keywords: swelling, liquid redistribution, shell stiffness, burst, porohyperelastic.

electrochemistry, and other factors. It also requires the consideration of the resistance between the liquid and solid constituents as they mechanically interact. Continuum mechanical treatments for this interactive seepage include well known and now classical works such as [Truesdell 1962; Bowen 1980] that remain highly recommended. More recent contributions that are also of a comprehensive nature include [Duda et al. 2010; Chester and Anand 2010; Pence 2012].

Because the present considerations restrict attention to equilibrated states where any liquid migration has ceased, the type of finite deformation treatment of swelling presented in [Tsai et al. 2004] may be applied. This type of treatment was employed in [Pence and Tsai 2006] for the study of swelling induced cavitation in spherical geometries. Here it is to be mentioned that the treatment of swelling in [Tsai et al. 2004; Pence and Tsai 2006] is, in certain aspects of its mathematical description, connected to treatments of growth and remodeling. Related work on cavitation under swelling/growth and its extension to include the effect of inclusions include [Goriely et al. 2010; Duda et al. 2011; Yavari and Goriely 2013; van der Sman 2015].

Balloon-like problems that make use of the constitutive models in [Tsai et al. 2004; Pence and Tsai 2006] for treating a spherical shell type wall were the focus of [Zamani and Pence 2017] where, among other things, a swelling induced abrupt burst phenomenon was examined. This burst phenomenon, like swelling induced cavitation, can be viewed as a more general example of swelling induced instability (see [Amar and Ciarletta 2010] for the effect of constraint on such instabilities). Recent related work on inflation instabilities and broader issues for spherical geometry problems that have connection to the treatment here are given in [Selvadurai and Suvorov 2018; Mihai et al. 2019; Cheng et al. 2019].

The continuum mechanical framework is presented in Section 2, including the formulation of the spherical inflation boundary value problem and a summary of the key results from [Zamani and Pence 2017] which was restricted to the consideration of uniform swelling. This section can also serve as a quick review of previous results. Section 3 gives the necessary modifications so as to treat nonuniform swelling distributions, and in particular introduces the class of harmonic swelling distributions. Section 4 then investigates the central question, which is how liquid redistribution affects the pressure-inflation behavior. It is found that, among other things, redistribution can lead to an overall change in the structural compliance. It can also change the basic monotonicity behavior of the pressure versus inflation graph. The consequences of these findings as it relates to possible expansion/contraction at fixed pressure, solely by liquid redistribution in the shell wall, are elaborated in Section 5. The final Section 6 places our findings in a broader perspective and discusses some of the main limitations in the overall approach.

2. Preliminaries

Swelling due to the infusion of liquid gives a local increase in volume. Because of this, the usual incompressiblity condition of volume preservation, $\det \boldsymbol{F} = 1$, where $\boldsymbol{F}$ is the deformation gradient, is generalized because of the volume change due to swelling. This yields

$$\det \boldsymbol{F} = v, \tag{1}$$

where v is the *swelling field*. Locations with $v = 1$ are unswollen (because no additional liquid is present), in which case the usual incompressibility constraint is recovered. Locations where $v > 1$ are swollen due to the presence of additional liquid whereupon v gives the new natural free volume (relative to the

unswollen reference state). It is to be remarked that the incompressible porous ground substance base constituent may itself contain irretrievably bound liquid in its fine microstructure. In such a case the liquid referred to in this treatment is in fact the free liquid (potentially mobile liquid), and the reference configuration then describes the porous base material with its bound liquid constituent (see e.g., [van der Sman 2015]).

As demonstrated in [Fang et al. 2008] in the context of polymer gels, and discussed in [Gou and Pence 2016] in the context of biological tissue, a treatment that employs (1) as a constraint, meaning that v as a function of location is specified, is appropriate when electrochemical effects (including osmotic pressure) dominate mechanical forces in the determination of equilibrium when an incompressible liquid constituent causes swelling in an otherwise incompressible porous ground substance constituent.

2.1. ***Hyperelastic stored energy.*** The material's mechanical response, both prior to swelling and after any swelling has occurred, is treated as hyperelastic. Let W be the elastic energy density as measured with respect to the unswollen reference configuration. As in hyperelasticity without swelling, this W is a function of the deformation gradient where frame invariance requires this dependence to be in terms of the right Cauchy–Green deformation tensor $\boldsymbol{C} = \boldsymbol{F}^T\boldsymbol{F}$. In addition, W will now also depend upon the liquid volume fraction as indicated in terms of the local amount of swelling v. This gives $W = W(\boldsymbol{C}, v)$. In the absence of body forces the equilibrium equation is $\operatorname{div}\boldsymbol{T} = 0$ where $\boldsymbol{T}$ is the Cauchy stress tensor:

$$\boldsymbol{T} = \frac{2}{v}\boldsymbol{F}\frac{\partial W}{\partial \boldsymbol{C}}\boldsymbol{F}^T - p\boldsymbol{I}. \tag{2}$$

Here p is the reactive stress associated with the constraint (1). It is a pure pressure contribution as in the conventional incompressible theory that is now generalized to include the liquid swelling effect.

We consider isotropic materials, in which case the dependence of W upon $\boldsymbol{C}$ is through the invariants of $\boldsymbol{C}$,

$$I_1 = \operatorname{tr}\boldsymbol{C}, \quad I_2 = \tfrac{1}{2}\big((\operatorname{tr}\boldsymbol{C})^2 - \operatorname{tr}\boldsymbol{C}^2\big). \tag{3}$$

The third isotropic invariant $I_3 = \det\boldsymbol{C} = v^2$ by virtue of (1). Consequently, $W = W(I_1, I_2, v)$ and this causes the $\boldsymbol{T}$ in (2) to take the form

$$\boldsymbol{T} = \frac{2}{v}\left(\frac{\partial W}{\partial I_1} + I_1\frac{\partial W}{\partial I_2}\right)\boldsymbol{B} - \frac{2}{v}\frac{\partial W}{\partial I_2}\boldsymbol{B}^2 - p\boldsymbol{I}. \tag{4}$$

Here $\boldsymbol{B} = \boldsymbol{F}\boldsymbol{F}^T$ is the left Cauchy–Green deformation tensor.

The particular constitutive model that we shall employ here takes the well known Mooney–Rivlin model in the classical incompressible theory and extends it to include the swelling effect [Treloar 1975]. For our purposes this motivates the form

$$W(I_1, I_2, v) = \frac{1}{2}\alpha\mu v^{q_1}\left(\frac{I_1}{v^{2/3}} - 3\right) + \frac{1}{2}(1-\alpha)\mu v^{q_2}\left(\frac{I_2}{v^{4/3}} - 3\right), \tag{5}$$

that was used in [Zamani and Pence 2017]. Here $\mu > 0$ is the infinitesimal shear modulus in the absence of swelling and α obeying $0 \le \alpha \le 1$ is the Mooney–Rivlin parameter that distinguishes between the I_1 and I_2 content of the material. The exponents q_1 and q_2 provide for a possible swelling sensitivity in the

I_1 to I_2 content ratio. Note that the conventional Mooney–Rivlin form is recovered upon setting $v = 1$. The neo-Hookean form is obtained by making the additional specialization $\alpha = 1$.

2.2. ***Spherical inflation.*** Using the above framework we consider a finite thickness spherical shell with inner radius $R_i > 0$ and outer radius $R_o > R_i$ prior to any loading or any swelling. Attention is restricted to radially symmetric swelling $v = v(R)$. The loading is taken to consist of applied pressures P_i and P_o on the inner and outer boundaries. These symmetric conditions motivate the consideration of the symmetric deformation for *radial inflation*

$$r = r(R), \quad \theta = \Theta, \quad \phi = \Phi, \tag{6}$$

on $R_i \le R \le R_o$, $0 \le \Theta < 2\pi$, $0 \le \Phi \le \pi$ where the radial inflation function $r(R)$ is to be determined. Thus (6) is a map from reference spherical coordinates (R, Θ, Φ) to deformed spherical coordinates (r, θ, ϕ). Let $\{\boldsymbol{e}_R, \boldsymbol{e}_\Theta, \boldsymbol{e}_\Phi\}$ and $\{\boldsymbol{e}_r, \boldsymbol{e}_\theta, \boldsymbol{e}_\phi\}$ represent unit basis vectors in the spherical coordinate system of the respective reference and deformed configurations. It follows from (6) that the deformation gradient is given by

$$\boldsymbol{F} = r'(\boldsymbol{e}_r \otimes \boldsymbol{e}_R) + \lambda(\boldsymbol{e}_\theta \otimes \boldsymbol{e}_\Theta + \boldsymbol{e}_\phi \otimes \boldsymbol{e}_\Phi), \tag{7}$$

with $r' = dr/dR$ and $\lambda = r/R$. Here λ is the azimuthal stretch, meaning that it is the stretch along spherical surfaces. Because of the spherical symmetry, the stretch λ is the same in all directions upon each spherical surface. However, λ will vary through the thickness of the shell. The swelling condition (1) becomes $v = \det \boldsymbol{F} = \lambda^2 r' = r^2 r'/R^2$, making $r' = v/\lambda^2$, and thus yielding

$$I_1 = \frac{v^2}{\lambda^4} + 2\lambda^2, \quad I_2 = \lambda^4 + 2\frac{v^2}{\lambda^2}. \tag{8}$$

Also, because $v = v(R)$, condition (1) in the form $r^2\, dr = vR^2\, dR$ integrates to

$$r^3 = r_i^3 + 3\int_{R_i}^{R} v(\zeta)\, \zeta^2\, d\zeta, \tag{9}$$

where $r_i = r(R_i)$ and ζ is a dummy integration variable. More generally (9) provides the map $r = r(R)$ in terms of the single parameter r_i which still needs to be determined.

It also follows from (4), (7) and the first of (8) that the Cauchy stress tensor takes the form

$$\boldsymbol{T} = T_{rr}(\boldsymbol{e}_r \otimes \boldsymbol{e}_r) + T_{\theta\theta}(\boldsymbol{e}_\theta \otimes \boldsymbol{e}_\theta + \boldsymbol{e}_\phi \otimes \boldsymbol{e}_\phi), \tag{10}$$

with

$$T_{rr} = -p + \frac{2v}{\lambda^4}\frac{\partial W}{\partial I_1} + \frac{4v}{\lambda^2}\frac{\partial W}{\partial I_2}, \tag{11}$$

$$T_{\theta\theta} = -p + \frac{2\lambda^2}{v}\frac{\partial W}{\partial I_1} + \left(\frac{2v}{\lambda^2} + \frac{2\lambda^4}{v}\right)\frac{\partial W}{\partial I_2}. \tag{12}$$

The specified pressures P_i and P_o at the inner and outer surfaces yield the boundary conditions

$$T_{rr}|_{r_i} = -P_i, \quad T_{rr}|_{r_o} = -P_o, \tag{13}$$

where $r_o = r(R_o)$. It is readily verified that the radial symmetry condition $p = p(R)$ leads to the satisfaction of the equilibrium equation along the θ and ϕ coordinate directions, leaving the radial equation

$$\frac{dT_{rr}}{dr} + \frac{2}{r}(T_{rr} - T_{\theta\theta}) = 0, \tag{14}$$

which is formally an ordinary differential equation for $p(R)$ because $d/dr = (1/r')d/dR = (r^2/vR^2)d/dR$. Because of (9) this first order differential equation contains the parameter r_i and for this reason is able to accommodate the two boundary conditions (13) by proper choice of that parameter. One is easily led to the equation for r_i by performing the relevant substitutions, integrating, and applying the boundary conditions.

In the absence of swelling, so that pressure is the only agent driving the deformation, this problem has a long and storied history in hyperelasticity going back at least to the work of Green and Shield [1950]. To make contact with that work set $v \equiv 1$ whereupon r_i is determined solely from the pressure difference between the interior and the exterior of the sphere:

$$\Delta P = P_i - P_o.$$

Much of the reason for the interest in that problem is that *inflation curves* of ΔP as a function of r_i may then exhibit nonmonotone behavior, even though the energy function W obeys relations, such as the Baker–Ericksen inequality, that are typically regarded as sufficient for physically realistic response. This leads to inflation instabilities, and there is a vast literature on the subject. A particularly elegant exposition is found in the work of Carroll [1987]. Generalizing that work to address the swelling effect in terms of the field variable v was one of the principal aims of [Zamani and Pence 2017].

For our purposes a useful and elegant procedure is obtained by rewriting $W(I_1, I_2, v)$ as $w(\lambda, v)$ upon making use of (8). Then note that

$$\frac{\partial w}{\partial \lambda} = \frac{\partial W}{\partial I_1}\frac{\partial I_1}{\partial \lambda} + \frac{\partial W}{\partial I_2}\frac{\partial I_2}{\partial \lambda} = 4\left(\lambda - \frac{v^2}{\lambda^5}\right)\frac{\partial W}{\partial I_1} + 4\left(\lambda^3 - \frac{v^2}{\lambda^3}\right)\frac{\partial W}{\partial I_2} = 2\frac{v}{\lambda}(T_{\theta\theta} - T_{rr}) = \frac{vr}{\lambda}\frac{dT_{rr}}{dr}, \tag{15}$$

where the last two steps employed first the pair (11) and (12) and then (14). The boundary conditions (13) now give

$$\Delta P = \int_{r_i}^{r_o} \frac{dT_{rr}}{dr}\, dr = \int_{R_i}^{R_o} \frac{\lambda}{vr}\frac{\partial w}{\partial \lambda}\frac{dr}{dR}\, dR, \tag{16}$$

whereupon again using $r' = v/\lambda^2$ and $\lambda = r/R$ we thus obtain

$$\Delta P = \int_{R_i}^{R_o} \frac{R}{r^2}\frac{\partial w}{\partial \lambda}\, dR. \tag{17}$$

An alternative form follows by noting that $R\, d\lambda/dR = -\lambda + v/\lambda^2$ which enables one to transform (17) into

$$\Delta P = \int_{\lambda_i}^{\lambda_o} \frac{1}{v - \lambda^3}\frac{\partial w}{\partial \lambda}\, d\lambda, \tag{18}$$

where $\lambda_i = r_i/R_i$ and $\lambda_o = r_o/R_o$ are the stretches at the inner and outer surface, respectively. All of these forms revert back to well known formulas in the absence of swelling ($v = 1$) and, just as in

those nonswelling treatments, alternative elegant means can be utilized to obtain these formulas, such as starting from a principal stretch formulation or pursuing an energy treatment.

Calculating the derivative $\partial w/\partial\lambda$ for the Mooney–Rivlin-type model (5) and inserting that form into (17) now provides

$$\frac{\Delta P}{\mu} = 2\int_{R_i}^{R_o} \frac{R}{r^2}\left[\alpha v^{q_1}\left(\frac{r}{Rv^{2/3}} - \frac{R^5 v^{4/3}}{r^5}\right) + (1-\alpha)v^{q_2}\left(\frac{r^3}{R^3 v^{4/3}} - \frac{R^3 v^{2/3}}{r^3}\right)\right] dR. \tag{19}$$

Here $v = v(R)$ is regarded as given and thus the general form of $r = r(R)$ follows from $v(R)$ using (9). This general form for $r(R)$ contains r_i as a parameter. As the parameter r_i is varied the integral (19) generates different values for the pressure difference ΔP. In this way the *pressure-inflation graph* for the given swelling field is determined.

2.3. ***Pressure-inflation relation in the absence of swelling.*** In the absence of swelling, the problem under consideration is a classical one that has been widely studied within the theory of incompressible finite hyperelasticity, i.e., with the constraint $\det \boldsymbol{F} = 1$. A radially symmetric spherical inflation is then possible in every isotropic homogeneous incompressible hyperelastic material. This gives rise to inflation graphs that follow from formulae such as (19) by simply taking $v \equiv 1$. The expectation that there is no inflation if $\Delta P = 0$ follows by noting that the integral (19) vanishes upon setting $v = 1$ and taking $r = R$. Thus inflation graphs in the absence of swelling "start" at $(r_i, \Delta P) = (R_i, 0)$.

As r_i increases from R_i it may be that the graph simply increases monotonically. This is called type-(a) behavior. However, the graph may also increase to a maximum and then monotonically decrease to zero; this is type-(b) behavior. Finally, the graph may first increases to a local maximum, then decrease to a local positive minimum before again monotonically increasing; this is type-(c) behavior. All three types of behavior can occur for the classical Mooney-Rivlin model energy (5) in the absence of swelling, as illustrated in Figure 1. In particular, for (5) with $v = 1$ this behavior is determined as follows: if $\alpha = 1$ then type-(b) behavior is ensured (this is the well known neo-Hookean material behavior). If $0 \le \alpha < 0.823$ then type-(a) behavior is ensured. With $0.823 < \alpha < 1$, type-(a) behavior occurs if the shell is thick, but type-(c) occurs if the shell is thin. Here thick and thin is determined in terms of the *shell thickness ratio* $\xi \equiv R_i/R_o$. There is a function $\xi_{a/c} = \xi_{a/c}(\alpha)$ that is monotonically decreasing on the interval $0.823 < \alpha < 1$ such that $\xi_{a/c}(0.823) = 1$ and $\xi_{a/c}(1) = 0$. For values $0.823 < \alpha < 1$, type-(a) behavior occurs if $R_i/R_o < \xi_{a/c}(\alpha)$ and type-(c) behavior occurs if $R_i/R_o > \xi_{a/c}(\alpha)$. Because $\xi_{a/c}(\alpha)$ is monotone, its inverse graph is also monotone, and the overall behavior can be summarized as shown in Figure 2.

Rivlin's experiments on gum rubber in the 1940s, which suggested that $\alpha \approx 7/8$ (for what was then known simply as the Mooney energy), in conjunction with nearly everybody's common experience in blowing up a party balloon, has mades this an intriguing (and well known) result in the theory of nonlinear elasticity. A balloon is thin walled (R_i/R_o close to one) and the common experience is that in blowing up a balloon there is first a clear amount of inflation resistance. However, at a certain pressure of blowing the previous inflation resistance suddenly gives way to an interval of easy inflation prior to a resumption of inflation resistance similar to the initial one. Connecting this abrupt and limited burst of inflation (not bursting in the sense of ultimate rupture, which is the balloon's sad fate if the pressure is increased

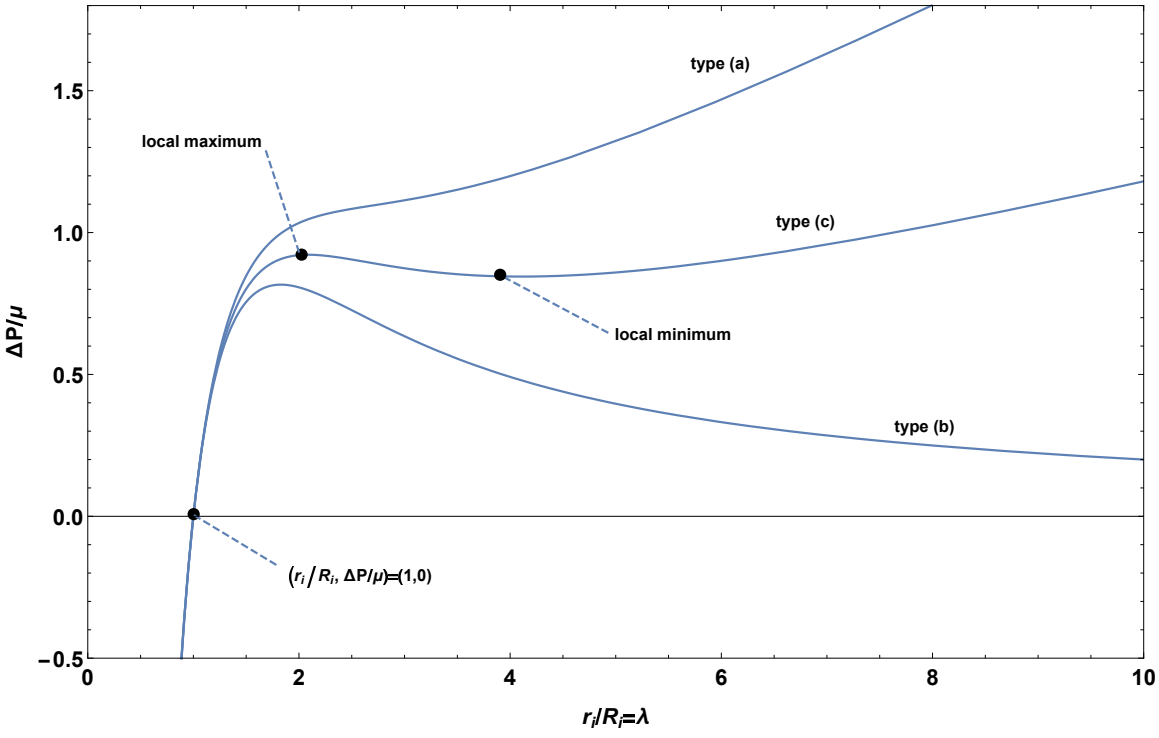

Figure 1. Inflation graphs showing three qualitatively different types of behavior (*a*)-(*c*) when there is no swelling ($v = 1$). These particular graphs correspond to W in (5), all with thickness ratio $R_i/R_o = 0.5$. The differences are due to the value of α. Here: $\alpha = 0.8$ (top curve); $\alpha = 0.9$ (middle curve); and $\alpha = 1$ (bottom curve).

too much) to the multivaluedness of r_i as a function of ΔP for type-(c) behavior, has generated an extensive literature — both experimental and theoretical (see e.g., [Müller and Strehlow 2004]).

A simple analtyical characterization of the equation describing the function $\xi_{a/c}(\alpha)$ in Figure 2 is not straight forward. Carroll [1987] has elegantly described the mathematical conditions that define this function for general hyperelastic stored energy functions $W(I_1, I_2)$. This permits an analytical characterization in terms of multiple functions and equations that we now briefly summarize. First define two functions $G(\eta)$ and $H(\eta, \xi)$ as

$$G(\eta) = \frac{1}{2}\eta^{2/3}\frac{\partial w}{\partial \lambda}\bigg|_{\lambda=\eta^{-1/3}}, \quad H(\eta, \xi) = G(x)|_{x=\eta/(\xi^3+\eta(1-\xi^3))}. \tag{20}$$

Here the function $w(\lambda)$ is as described above just before (15) with the additional specialization of taking $v = 1$ since Carroll [1987] did not seek to treat swelling. The condition for a value ξ to be on the transition curve (the curve labelled $\xi_{a/c}$ in Figure 2) is that it gives the simultaneous satisfaction of the two equations

$$G(\eta) = H(\eta, \xi), \quad \frac{\partial G}{\partial \eta} = \frac{\partial H}{\partial \eta}. \tag{21}$$

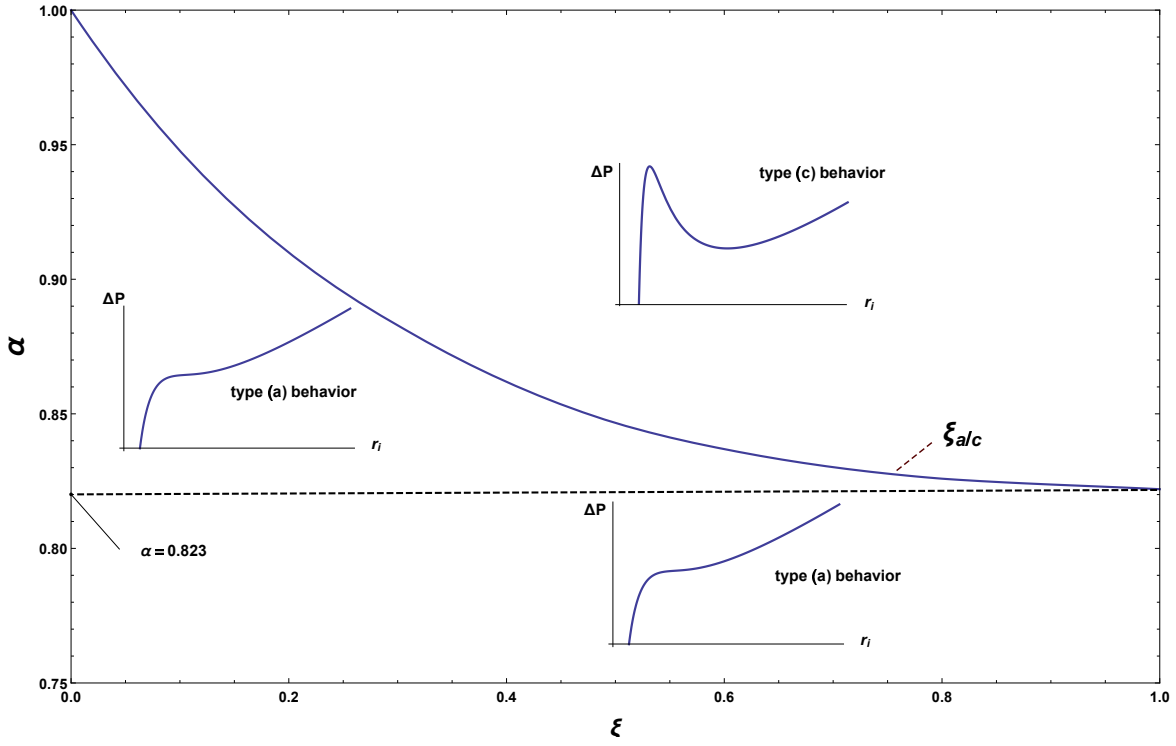

Figure 2. Qualitative behavior of the inflation graph for the Mooney–Rivlin model W given by (5) in the absence of swelling ($v = 1$). The curve $\xi = \xi_{a/c}$ provides a transition between type-(c) and type-(a) behaviors.

For the Mooney–Rivlin energy the function $G(\eta)$ is given by

$$G(\eta) = \mu\big[\alpha\big(\eta^{1/3} - \eta^{7/3}\big) + (1-\alpha)\big(\eta^{-1/3} - \eta^{5/3}\big)\big].$$

The $\xi_{a/c}$ curve in Figure 2 can then be constructed numerically by ranging through the values of ξ in the interval $0 < \xi < 1$ and in each case eliminating η between the two equations in (21) while solving for α.

For type-(c) behavior, because the first monotonically increasing "branch" of the graph terminates at the local maximum, an increasing ΔP then necessitates some kind of "branch transition" (again, the party balloon). There is an interval of ΔP on which this transition (i.e., jump) can in principle take place, and different physically based criteria can select different transition values of ΔP. In particular, a maximum delay criterion (which invokes the jump when the current branch "runs out") is suggested by energy minimization with respect to weak variations. Alternatively, the "Maxwell line" convention, based on the equal area rule with respect to the inflation graph, is suggested by energy minimization with respect to strong variations. Other conventions are also possible (based, for example, on thermodynamic fluctuations, or additional physical effects that may enter). We return to these considerations later in Section 5.

2.4. ***Pressure-inflation relation for uniform swelling.*** Building on the analysis of [Carroll 1987] our work [Zamani and Pence 2017] considered various aspects of uniform swelling as it relates to this problem

of spherical inflation. This means that v is independent of R. One of the main issues addressed in [Zamani and Pence 2017] was the inflation behavior as this uniform v varied with time in a quasistatic fashion. Thus, ΔP and v served as independent load-type parameters. Attention was restricted to $v \geq 1$, since "de-swelling" (or dessication) would generally lead to various wrinkling type instabilities that were not in the scope of that work. Also, because v was uniform, the relation (18) was relatively easy to use, and it became a central focus of the analysis in [Zamani and Pence 2017].

The pressure-inflation graphs remain a useful tool, as does the (a)–(c) classification type for those graphs. Now the graphs depend upon v. In other words, *there is a separate graph for each* $v \geq 1$. Note then that the homogeneous deformation of uniform expansion $r = v^{1/3}R$ makes $\Delta P = 0$ as can be verified directly from (19) and which also can be shown to follow from (18). Thus we have the intuitive result that uniform swelling gives uniform expansion when $\Delta P = 0$. In other words, the pressure inflation graphs for uniform swelling v now "start" at $(r_i, \Delta P) = (v^{1/3}R_i, 0)$.

Much of the technical analysis in [Zamani and Pence 2017] is based on a swelling generalization of Carroll's treatment in terms of an appropriate generalization of the G and H functions that appear in (20). One of the main results from that treatment is that if $q_1 = q_2$ in (5) then the value of v does not affect the behavior type (a)–(c). Thus, Figure 2 continues to indicate the qualitative form of the inflation graph for any uniform v provided that $q_1 = q_2$. On the other hand, it was also established that if $q_1 \neq q_2$ then the behavior type could vary with v. Thus, if $q_1 \neq q_2$, an unswollen inflation graph might have type-(a) behavior, whereas uniform wall swelling $v > 1$ might cause the inflation graph to become one with type-(c) behavior. This has obvious consequences for swelling induced instability phenomena. Qualitatively describing and quantitatively characterizing those consequences was a major focus in [Zamani and Pence 2017]. In fact, as described in that work, it is also possible to get limited burst type instability phenomena from swelling, even if the graph type did not change with v (e.g., even if $q_1 = q_2$). A rather complete mathematical framework for addressing the various possibilities was presented in [Zamani and Pence 2017], where, again, only uniform swelling was considered.

3. Nonuniform harmonic swelling fields

Turning to the main new issue of interest, we wish to consider the effect of nonuniform swelling fields. As previously mentioned, the spherical symmetry is maintainable so long as $v = v(R)$. For each such $v(R)$ the determination of the inflation graph continues as a key consideration, and it remains useful to classify their behavior according to the (a)–(c) scheme. However, when v is nonuniform, any use of the relation (18) necessitates expressing v as a function of λ. In the event that such a function is not single valued, then the integral must be split up into various λ ranges. For this reason, it is simpler to work directly with (19) which is the course followed for the rest of this paper.

On this basis, as we establish in the remainder of this paper, the behavior type according to the (a)–(c) scheme does not as directly correlate with the parameters in W as it did for the case of uniform swelling. For example, whereas W in (5) with $q_1 = q_2$ allowed for the continued use of Figure 2 for uniform swelling, Figure 2 will no longer determine the behavior type if $v(R)$ is not uniform even if $q_1 = q_2$.

Since our interest is in different nonuniform swelling fields $v(R)$, all of which correspond to the same amount of movable liquid, it is useful to introduce ΔV the *added swelling volume* associated with the

swelling field $v(R)$. Thus

$$\Delta V = 4\pi \int_{R_i}^{R_o} (v(R) - 1) R^2 dR. \tag{22}$$

In particular, because the swelling is due to an original soft hyperelastic ground substance having imbibed a certain amount of incompressible liquid, it follows that ΔV represents the combined volume of all of this free and potentially movable liquid. In the mathematical treatment, it is then natural to encounter the nondimensionalized quantity $\Delta V / R_i^3$.

The interpretation of ΔV in terms of the added mass of an incompressible fluid swelling agent gives rise to the key question of the present study: what changes in mechanical behavior take place if the same amount of liquid simply redistributes itself within the shell wall in different ways? Examining this question serves as the guiding principle for the remainder of this inquiry.

On this basis, we seek to consider various functions $v(R)$, all of which have a common $\Delta V > 0$. Even with this restriction, the problem remains rather general and so attention is further restricted to functions $v(R)$ of the special form

$$v(R) = \frac{A}{R} + B, \tag{23}$$

where A and B are constants. The form (23) is chosen here because this makes $v(R)$ the general spherically symmetric solution to $\nabla^2 v = 0$. From a physical perspective, one may then contemplate a variety of physical mechanisms that might suggest such a "harmonic form". For example, chemical potential regulation at the inner and outer radii for the purpose of establishing an osmotic pressure gradient might possibly suggest such a scenario, although we do not here seek to tie the ensuing results to this or any other particular mechanism.

Entering (22) with (23) one obtains

$$\frac{\Delta V}{R_i^3} = \frac{2\pi}{R_i}(\xi^{-2} - 1)A + \frac{4\pi}{3}(\xi^{-3} - 1)(B - 1), \tag{24}$$

where ξ obeying $0 < \xi < 1$ continues to be the ratio R_i / R_o. In working with (23) and (24) let

$$v_i \equiv v(R_i) = \frac{A}{R_i} + B, \quad v_o \equiv v(R_o) = \frac{A}{R_o} + B, \tag{25}$$

which means that v_i is the local swelling amount at $R = R_i$ and v_o is the local swelling amount at $R = R_o$. It then follows that

$$A = \frac{v_o - v_i}{1/R_o - 1/R_i}, \quad B = \frac{v_o R_o - v_i R_i}{R_o - R_i}. \tag{26}$$

It will be convenient to characterize the distributions (23) in terms of ΔV and the parameter v_i, instead of A and B. To this end, enter (24) with (26) and solve for v_o, which gives

$$v_o = \frac{3\Delta V}{2\pi R_i^3}\left(\frac{\xi^3}{(1-\xi)(2+\xi)}\right) - \frac{\xi(1+2\xi)}{2+\xi} v_i + \frac{2(1+\xi+\xi^2)}{2+\xi}, \tag{27}$$

whereupon

$$A = \left[-\frac{3\Delta V}{2\pi R_i^3}\left(\frac{\xi^3}{2-3\xi+\xi^3}\right) + v_i\left(\frac{2(1-\xi^3)}{2-3\xi+\xi^3}\right) - \frac{2(1-\xi^3)}{2-3\xi+\xi^3}\right] R_i,$$
$$B = \frac{3\Delta V}{2\pi R_i^3}\left(\frac{\xi^3}{2-3\xi+\xi^3}\right) - v_i\left(\frac{3\xi(1-\xi^2)}{2-3\xi+\xi^3}\right) + \frac{2(1-\xi^3)}{2-3\xi+\xi^3}. \tag{28}$$

Thus for a given $\Delta V > 0$, R_i, and $R_o = R_i\,\xi^{-1}$ we may view (23) with A and B given by (28) as a family of harmonic swelling fields, each with the same overall free liquid content but with different distributions of that liquid as determined by the single "tuning parameter" v_i. As v_i changes, the same overall added mass ΔV due to the fixed amount of liquid swelling agent is distributed through the spherical shell in different ways.

We restrict considerations to swelling fields (23) such that $v(R) \geq 1$ at all locations. This will be the case if both $v_i \geq 1$ and $v_o \geq 1$. Setting $v_o = 1$ in (27) and solving for v_i yields

$$v_i|_{v_o=1} = 1 + \frac{3\Delta V}{2\pi R_i^3}\left(\frac{\xi^2}{1+\xi-2\xi^2}\right) \equiv v_i^{\max}. \tag{29}$$

Thus, (23) with A and B given by (28) is parameterized by v_i on the interval $1 \leq v_i \leq v_i^{\max}$.

If $v_o = v_i$, then $A = 0$ and we retrieve a uniform distribution of the kind studied in [Zamani and Pence 2017]. For a given ΔV the uniform distribution is associated with the v_i value that is found by substituting $v_i = v_o = v_{\text{uni}}$ in (27) and solving for the special value v_{uni}. This gives

$$v_{\text{uni}} = 1 + \frac{3\Delta V}{4\pi R_i^3}\left(\frac{\xi^3}{1-\xi^3}\right). \tag{30}$$

If for a given added volume ΔV, the value v_i is exactly v_{uni} in (30), then the distribution is uniform and all of the results from [Zamani and Pence 2017] apply for the given added mass ΔV. Inverting (30):

$$\frac{\Delta V}{R_i^3} = \frac{4}{3}\pi(v_{\text{uni}} - 1)\frac{1-\xi^3}{\xi^3}, \tag{31}$$

and substituting from this result into (29) gives $v_i^{\max}$ in terms of v_{uni} as

$$v_i^{\max} = 1 + 2(v_{\text{uni}} - 1)\frac{1+\xi+\xi^2}{\xi(1+2\xi)}. \tag{32}$$

Consequently, it follows that

- if $v_{\text{uni}} < v_i \leq v_i^{\max}$ then the added mass is more concentrated at the inner surface, and
- if $1 \leq v_i < v_{\text{uni}}$ then the added mass is more concentrated near the outer surface.

Figure 3 shows such a family of harmonic swelling distributions, all with the same overall added mass, which in this case is 30 percent of the original volume. Consequently, $v_{\text{uni}} = 1.3$. The value of $v_i^{\max}$ is dependent on ξ by virtue of (32). For Figure 3 we take the moderately thick wall $R_i = R_o/2$ or $\xi = 0.5$, which in turn makes $v_i^{\max} = 2.05$.

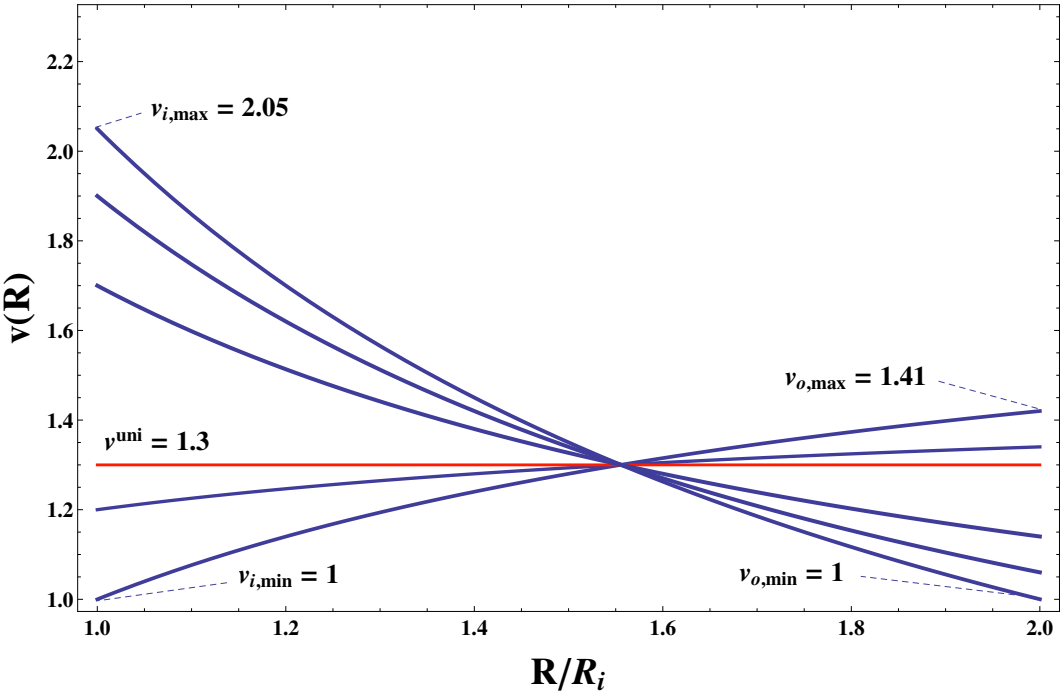

Figure 3. The family of harmonic swelling distributions (23) with constants (28) that are parameterized with respect to v_i such that $v(R) \geq 1$. Here $\xi = 0.5$. All distributions have the same amount of overall added mass associated with $v_{\text{uni}} = 1.3$ (30% increase in wall volume from the reference configuration that contains no free liquid).

4. Behavior under nonuniform swelling

The relations (29) and (30) show that the dependence of both $v_i^{\max}$ and v_{uni} upon $\Delta V/R_i^3$ is linear; also the resulting curve for $v_i^{\max}$ is above that for v_{uni}. Figure 4 shows these curves when $\xi = 0.9$. Vertical line segments in Figure 4 between $v_i = 1$ and $v_i = v_i^{\max}$ correspond to different harmonic swelling distributions for the same ΔV. In other words *each point on the vertical segment represents a harmonic swelling field, and the vertical segment itself encompasses all harmonic swelling fields for the fixed* ΔV. Consequently, the vertical line segment represents *a family of harmonic swelling fields*, and each member of the family involves a different distribution of the given amount of swelling agent.

The question now arises as to how the inflation graphs vary — if at all — as the swelling field changes within any such family. The physical significance is that if the inflation graphs are found to vary, then liquid redistribution will alter the inflation response.

The development thus far is capable of addressing a wide range of hyperelastic swelling material constitutive models; for material model (5) this range is characterized by choices for μ, α, q_1 and q_2. The development also addresses spherical shells of different wall thickness ratios $\xi = R_i/R_o$. For the purpose of illustrating the rich range of behaviors that can occur we provide results in the context of the material model (5) with $\alpha = 0.85$, $q_1 = q_2 = 0$ and a spherical shell with $\xi = 0.9$. The value $\alpha = 0.85$ is motivated by the previously indicated Rivlin experiments and the values $q_1 = q_2 = 0$ are

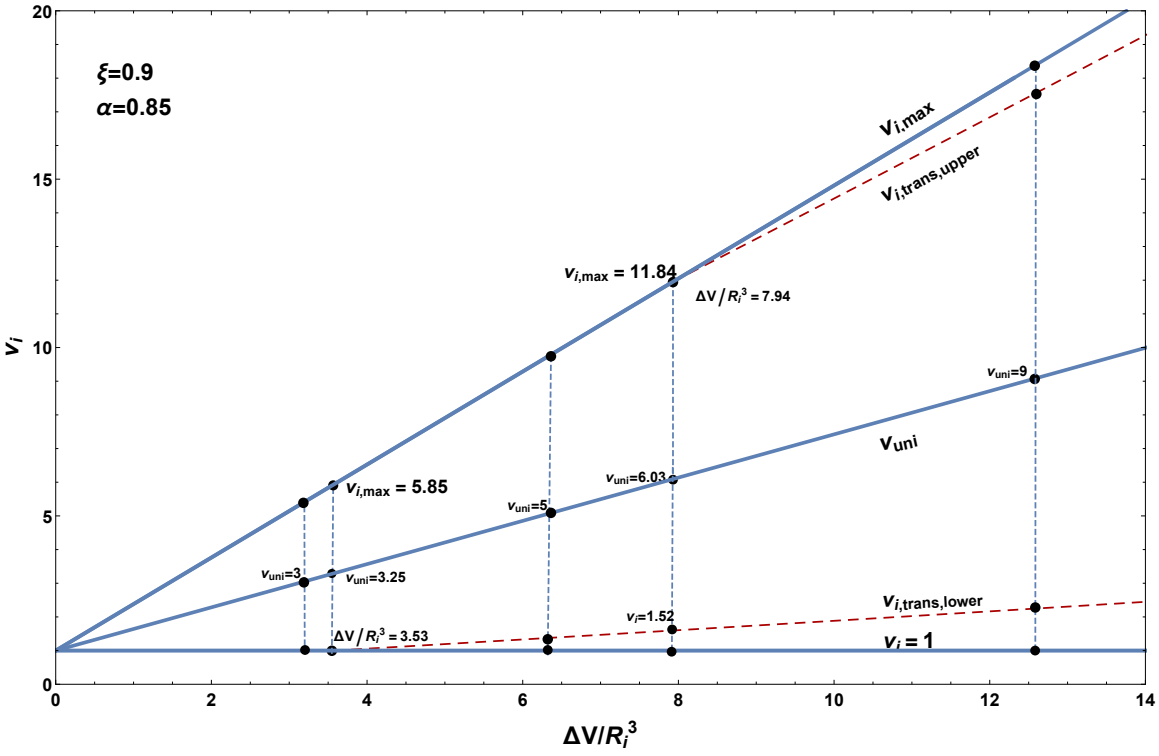

Figure 4. The value v_i on the interval $1 \le v_i \le v_i^{\max}$ parameterizes harmonic swelling fields, all of which have the same added mass content ΔV. For a given value of ΔV each of these parameterized families correspond to a vertical line segment on this figure, which here is for $\xi = 0.9$. The significance of the other curves is developed throughout the text narrative of Section 4.

broadly consistent with Treloar's remarks on swelling in [Treloar 1975]. The value $\xi = R_i/R_o$ gives a moderately thin bladder wall, but one in which internal redistribution of liquid would seem possible. Summarizing, we present results for

$$\frac{1}{\mu}W(I_1, I_2, v) = 0.425\frac{I_1}{v^{2/3}} + 0.075\frac{I_2}{v^{4/3}} - 1.5, \qquad R_i = 0.9R_o. \tag{33}$$

The shear modulus parameter μ then remains the scale parameter for the pressure. In this context, different amounts ΔV of liquid swelling agent are considered. Each value of ΔV gives rise to its own harmonic family of swelling fields, each of which is characterized by a different value of v_{uni} and $v_i^{\max}$ on the basis of (30) and (29) using $\xi = 0.9$.

Figures 5 and 6 show that the inflation graphs do indeed vary within a family. These two figures are for the case $\Delta V/R_i^3 = 3.20$, which makes $v_{\text{uni}} = 3$ and $v_i^{\max} = 5.3$. Figure 5 displays the inflation graphs for all values v_i on the interval $1 \le v_i \le 3.21$, whereas Figure 6 is for the remaining interval $3.21 \le v_i \le 5.3 = v_i^{\max}$. Each inflation graph in both figures is of type-(c). For Figure 5 we find that the uppermost inflation graph is that associated with $v_i = 1$. Then as v_i increases the graphs become

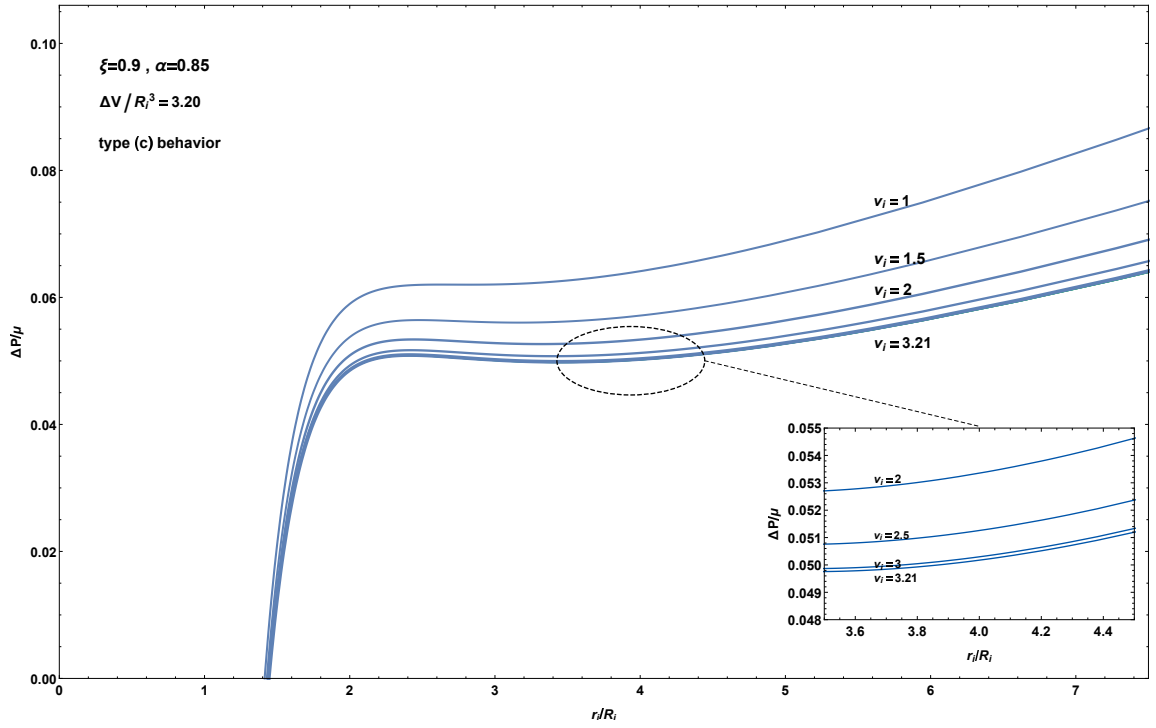

Figure 5. Inflation graphs for (33) with $\Delta V/R_i^3 = 3.20$ (which makes $v_{\text{uni}} = 3.0$ and $v_i^{\max} = 5.3$). The graphs here correspond to $1 \le v_i < 3.21$ which is the subfamily (of the overall family $1 \le v_i \le 5.3$) for which the graphs become lower as v_i increases.

progressively lower until reaching the lowermost graph corresponding to $v_i = 3.21$, thereby finishing Figure 5. Further increase in v_i then results in inflation graphs that become progressively higher as v_i continues to increase, all the way to the value $v_i^{\max} = 5.3$. These are shown in Figure 6. Thus the family of inflation graphs is effectively divided into two subfamilies: one for $1 \le v_i < 3.21$ and another for $3.21 < v_i \le 5.3 = v_i^{\max}$.

The lowest of all the graphs is found to occur when $v_i = 3.21$ which is close to the value $v_{\text{uni}} = 3$ where the swelling agent is uniformly distributed. It is to be noted from Figure 5 that the graph for the two curves $v_i = 3$ and $v_i = 3.21$ are quite close, so that it is not completely clear how numerical sensitivity might be a factor in this finding. In any event, the uniform distribution generates what is essentially the lowest graph in the overall family. Consequently, if the same amount of added mass is distributed in a highly nonuniform fashion, then to obtain the same inflation r_i requires a greater amount of pressure. In this sense an essentially uniform distribution of the swelling agent gives the most compliant response. By shifting more and more of the swelling agent to the wall extremities, one makes the response increasingly stiff. The stiffest response occurs when the mass is maximally concentrated at the outer surface of the wall (i.e., $v_i = 1$). By maximally concentrated, we mean within the class of harmonic swelling distributions that make $v(R) \ge 1$ for all R.

Figures 5 and 6 represented the family of inflation graphs for the particular added mass amount $\Delta V/R_i^3 = 3.20$. We now inquire into whether these graphs are representative when one considers other

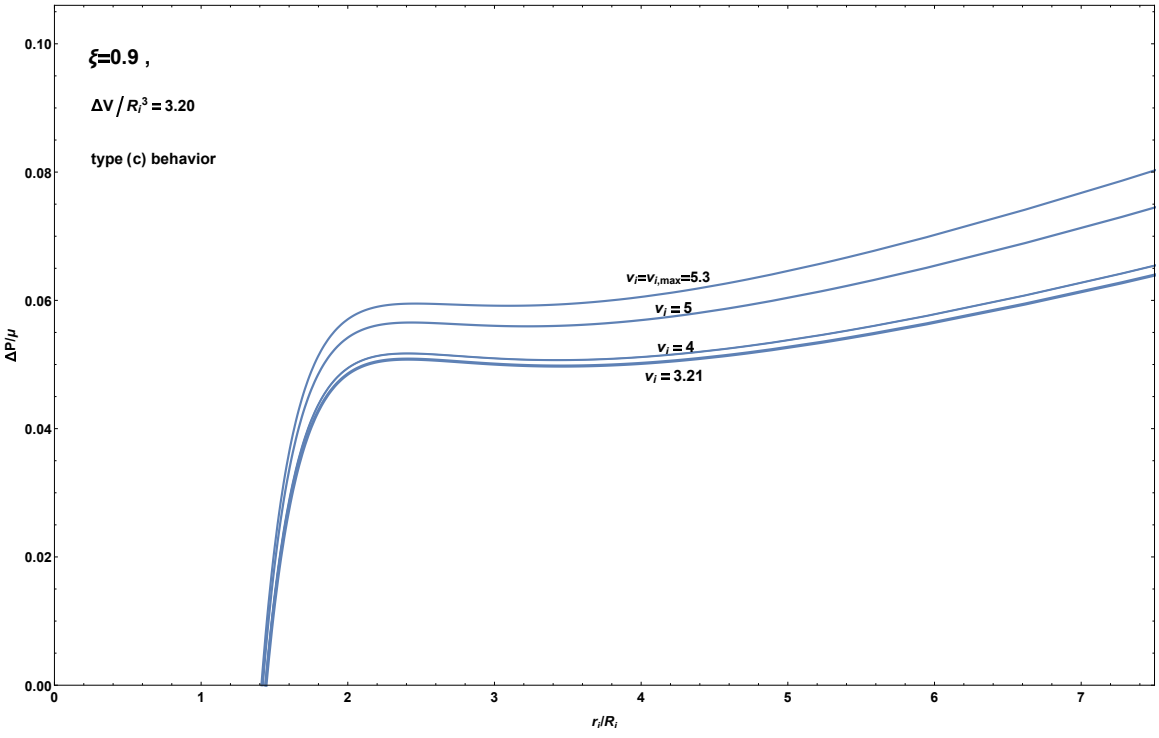

Figure 6. Subfamily of inflation graphs for (33) with $\Delta V/R_i^3 = 3.20$ corresponding to $3.21 < v_i \leq 5.3 = v_i^{\max}$. The complete family of inflation graphs $1 \leq v_i \leq v_i^{\max}$ is accounted for by combining these graphs with those from Figure 5.

values of $\Delta V/R_i^3$. In other words, we ask whether the general family behavior indicated in Figures 5 and 6 persists when one considers different vertical line segments in Figure 4? A partial answer to this question is provided by Figure 7 which corresponds to $\Delta V/R_i^3 = 6.36$ (making $v_{\text{uni}} = 5$ and $v_i^{\max} = 9.60$). Now we show the full family of graphs $1 \leq v_i \leq v_i^{\max}$ on the same figure. The lowest graph in Figure 7 is for $v_i = 5.43$ and it is again the case that the overall family is split into two subfamilies: the subfamily $1 \leq v_i < 5.43$ where the graphs become progressively lower, and the subfamily $5.43 < v_i \leq 9.60 = v_i^{\max}$ where they become progressively higher. As was the case for Figures 5 and 6, near the lowermost v_i-graph one finds that the nearby graphs become highly bunched together. Indeed the determination of the specific v_i-value of the lowest graph is sensitive to the numerical algorithm. Also, v_{uni} is again in the bunched region (see the inset in Figure 7).

As we examine other families (i.e., other values of $\Delta V/R_i^3$) we find that this general ordering behavior persists, namely there is a subfamily where the graphs become progressively lower followed by a rising subfamily. The lowermost graphs are highly bunched together near v_{uni}. Because of possible numerical sensitivity in this extreme bunching region, we shall henceforth regard v_{uni} as representative of the lowermost graph in the overall harmonic family of distributions.

Turning now from the graph ordering to the graph behavior in Figure 7 we find that the lowermost graph is again of type-(c). For the full family of graphs as parameterized by v_i on $1 \leq v_i \leq 9.60 = v_i^{\max}$,

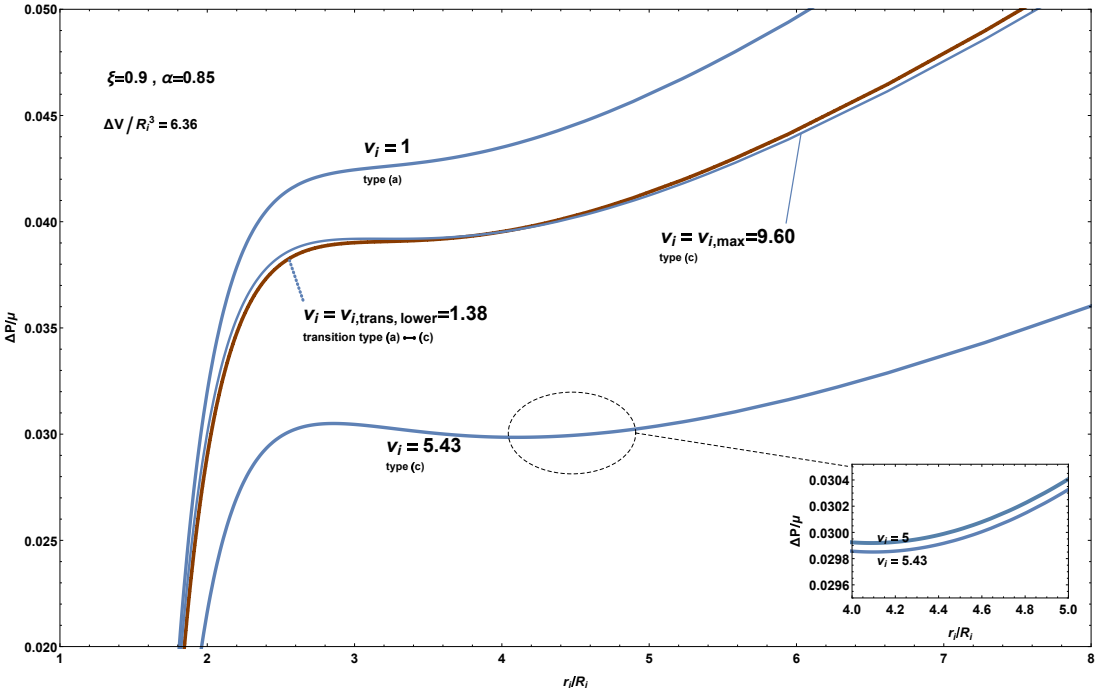

Figure 7. The family of inflation graphs for (33) with $\Delta V/R_i^3 = 6.36$ (which makes $v_{\text{uni}} = 5.0$ and $v_i^{\max} = 9.60$). Some remain type-(c) but others are now type-(a). The transition between the two behaviors is the particular inflation graph for $v_i = v_{i,\text{trans,lower}}$ which is shown in red.

we find that the bounding values $v_i = 1$ and $v_i = v_i^{\max}$ give different graph type behavior. Specifically, it is found that the graph for $v_i = v_i^{\max}$ is of type-(c), whereas the graph for $v_i = 1$ is of type-(a). All of the inflation graphs for $5.43 \leq v_i \leq v_{i,\max}$ are type-(c). As regards the range $1 \leq v_i < 5.43$ we find that that there is a special value of v_i in this range — which we here denote by the name $v_{i,\text{trans,lower}}$ — such that the inflation graph is of type-(a) for $1 \leq v_i < v_{i,\text{trans,lower}}$ and is of type-(c) for $v_{i,\text{trans,lower}} < v_i \leq v_{i,\max}$. In particular we find that $v_{i,\text{trans,lower}} = 1.38$.

Because figures 5 and 6 for $\Delta V/R_i^3 = 3.20$ show all type-(c) behavior whereas Figure 7 for $\Delta V/R_i^3 = 6.36$ shows both type-(c) and type-(a) behavior, we enquire into the transition between these two different sorts of families. In doing so we find that the special value $\Delta V/R_i^3 = 3.53$ provides the transition. For $\Delta V/R_i^3 < 3.53$ every member of the response curve family exhibits type-(c) behavior, whereas for $\Delta V/R_i^3 > 3.53$ both type-(c) and type-(a) behavior are found to occur. Figure 8 shows the family of inflation graphs for $\Delta V/R_i^3 = 3.53$. With the exception of the inflation graph for $v_i = 1$, all of the inflation graphs give type-(c) behavior and so have two locations with zero slope. For $v_i = 1$ in Figure 8 these two zero slope locations have coalesced giving a single zero slope location that is also an inflection point, which is the hallmark for the transition between the two different behavior types. In other words the value $v_{i,\text{trans,lower}}$ emerges from the value $v_i = 1$ when $\Delta V/R_i^3 = 3.53$.

Figure 4 also shows the vertical line corresponding to this transition family $\Delta V/R_i^3 = 3.53$. We then show the line in Figure 4 corresponding to $v_i = v_{i,\text{trans,lower}}$ for all $\Delta V/R_i^3 > 3.53$.

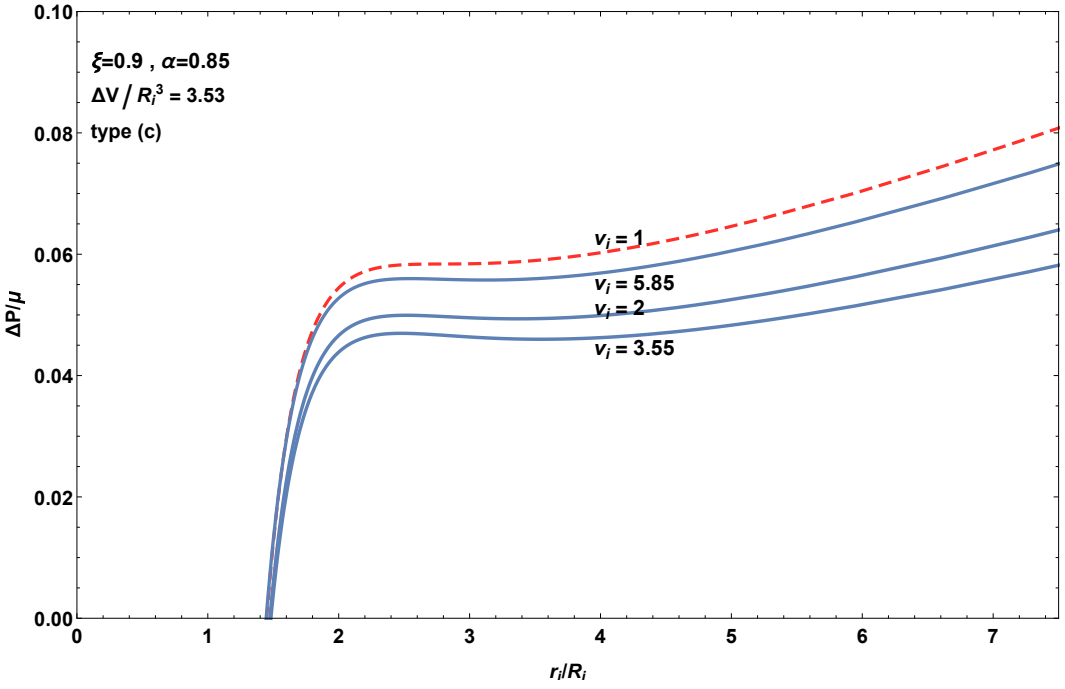

Figure 8. The family of inflation graphs for (33) with $\Delta V/R_i^3 = 3.53$ (which makes $v_{\text{uni}} = 3.25$ and $v_i^{\max} = 5.85$). The value $\Delta V/R_i^3 = 3.53$ provides the transition between the family type shown in figures 5 and 6 (always type-(c)) and the family type shown in Figure 7 (sometimes type-(c) and sometimes type-(a)).

This might seem to provide a full resolution to the issue of how the different inflation graph families for $\xi = 0.9$ and $\alpha = 0.85$ vary with overall swelling matter content ΔV. However, the consideration of even larger values of ΔV indicate that there is more to the story. Figure 9 shows the family of inflation graphs for $\Delta V/R_i^3 = 12.58$ (or $v_{\text{uni}} = 9$). As for all of the previous values of ΔV, the lowest inflation graph is either at or near the uniform distribution and this graph is of type-(c). Also, as in Figure 7, values of v_i sufficiently close to $v_i = 1$ give inflation graphs with type-(a) behavior. Now, however, it is also found that values of v_i sufficiently close to $v_i = v_{i,\max}$ also give type-(a) behavior. In other words, there are now (at least) two transitions away from the type-(c) behavior of the uniform distribution; one (or more) occurring for $v_i < v_{\text{uni}}$ and one (or more) occurring for $v_i > v_{\text{uni}}$. In fact, we find that there is one transition on each side of v_{uni}. The one for $v_i < v_{\text{uni}}$ is the previously found transition that occurs at $v_i = v_{i,\text{trans,lower}}$. The one for $v_i > v_{\text{uni}}$ is new and is now denoted by $v_{i,\text{trans,upper}}$. For the case of Figure 9, where $v_{\text{uni}} = 9$ and $v_i^{\max} = 18.2$, it is found that $v_{i,\text{trans,lower}} = 2.23$ and $v_{i,\text{trans,upper}} = 17.54$. The inflation graphs at both $v_{i,\text{trans,lower}}$ and $v_{i,\text{trans,upper}}$ have a single location with zero slope that is also an inflection point.

For all of the cases of very large ΔV that we have examined for $\xi = 0.9$ and $\alpha = 0.85$, we find that the general properties within the family of inflation curves qualitatively reflect that just described for the case of $\Delta V/R_i^3 = 12.58$ as depicted in Figure 9. The demarcation between the qualitative behavior of Figure 9 and the earlier qualitative behavior of Figure 7 (where there was only one transition between

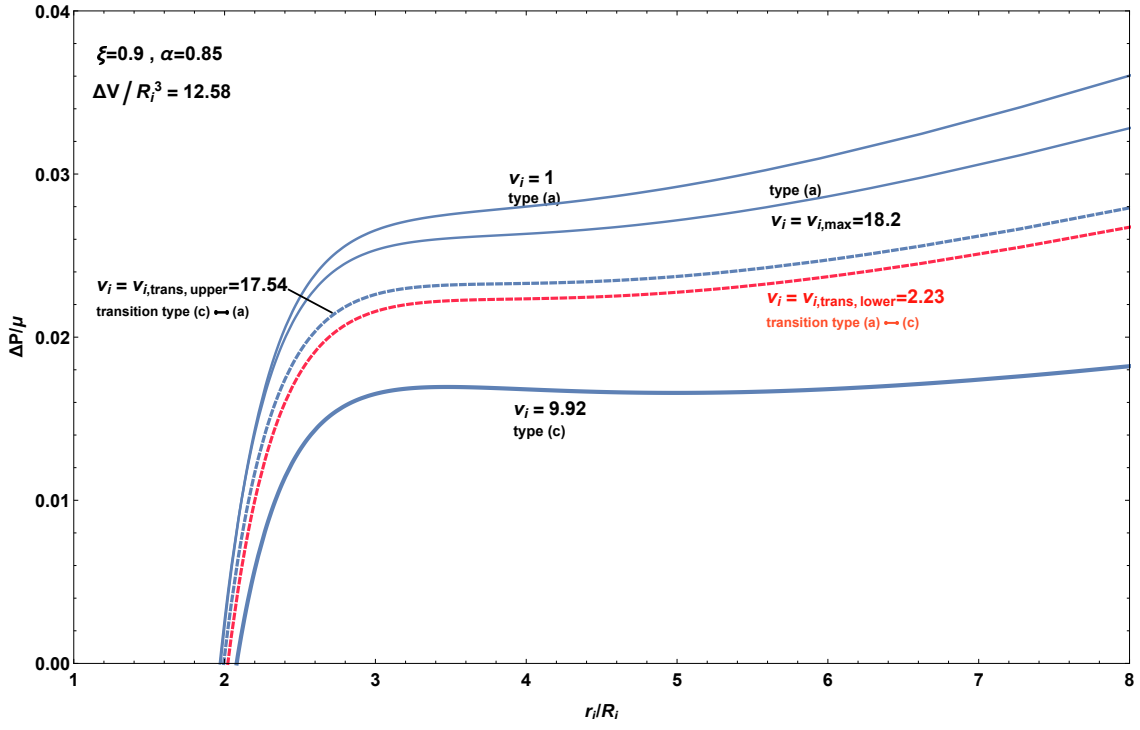

Figure 9. The family of inflation graphs for (33) with $\Delta V/R_i^3 = 12.58$ (which makes $v_{\text{uni}} = 9.0$ and $v_i^{\max} = 18.2$). Now the behavior is type-(c) for v_i near v_{uni} but type-(a) both near $v_i = 1$ and near $v_i = v_i^{\max}$.

type-(c) and type-(a) behavior) is found to occur at $\Delta V/R_i^3 = 7.94$. The corresponding family of inflation graphs for $\Delta V/R_i^3 = 7.94$ is depicted in Figure 10. This gives a case where $v_{i,\text{trans,upper}}$ first makes an appearance. Now, however, the emergence of this transition value occurs from $v_i = v_{i,\max}$ and not from $v_i = 1$ as was the case with the emergence of $v_{i,\text{trans,lower}}$. The emergence of $v_{i,\text{trans,upper}}$ from $v_{i,\max}$ is also depicted in Figure 4.

Based on all of the above considerations, Figure 4 now provides a complete picture of how the various type-(c) and type-(a) behaviors are organized. The swelling distributions as parameterized by v_i give rise to the region between the curves $v_i = 1$ and $v_i = v_{i,\max}$. The uniform distribution curve runs through the middle of this region. Above the uniform distribution curve, the swelling agent is more concentrated near the inner surface of the shell wall. Below the uniform distribution curve, the swelling agent is more concentrated near the outer surface of the shell wall. Type-(a) behavior occurs in two regions of Figure 4, one of which corresponds to a heavy concentration near the inner surface and the other of which corresponds to a heavy concentration near the outer surface. The central portion of the region containing the uniform distribution curve gives type-(c) behavior.

How can we so definitively assert that the uniform distribution curve is always in the type-(c) region of Figure 4? Alternatively stated, how do we know that both the curves for $v_{i,\text{trans,lower}}$ and $v_{i,\text{trans,upper}}$ remain bounded away from the uniform distribution curve? This is a consequence of a mathematical result obtained in [Zamani and Pence 2017]. That paper was solely devoted to uniform swelling distributions.

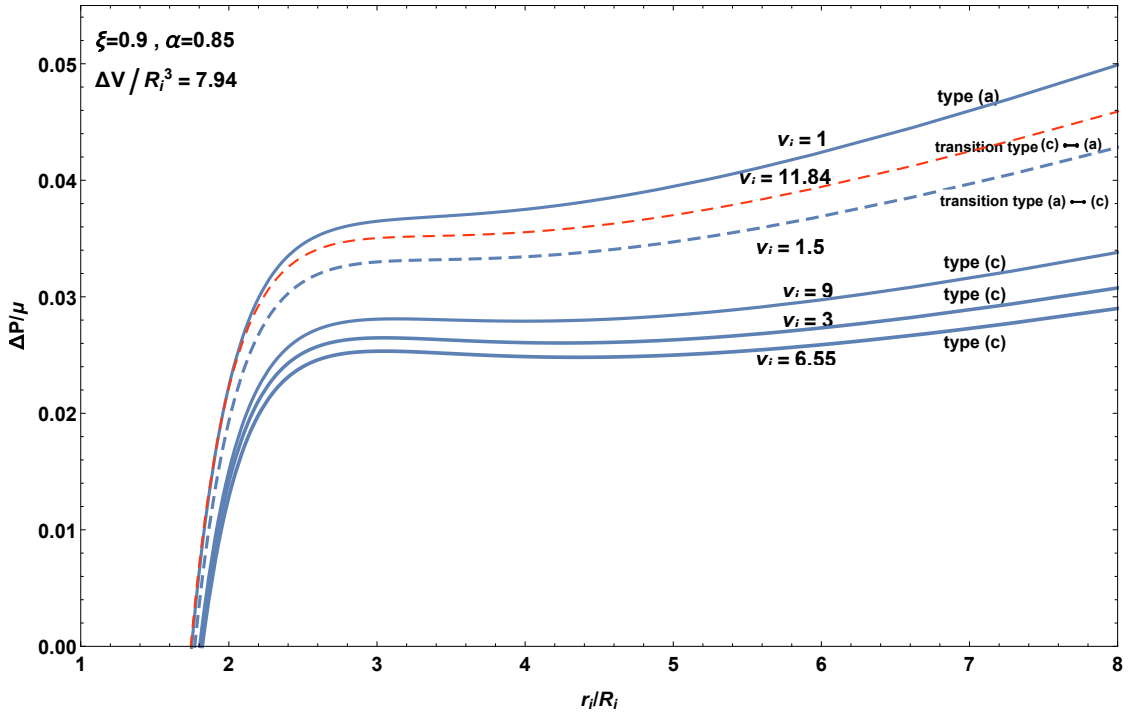

Figure 10. The family of inflation graphs for (33) with $\Delta V/R_i^3 = 7.94$ (which makes $v_{\text{uni}} = 6.03$ and $v_i^{\max} = 11.84$). The value $\Delta V/R_i^3 = 7.94$ provides the transition between the family types shown in figures 7 and 9.

As alluded to in Section 2.4, a key result of that work (see also [Pence and Tsai 2006]) was that a uniform swelling distribution does not alter the behavior type from that which is found in the treatment when no swelling is present. This rather general result ensures that the v_{uni} line in Figure 4 is always associated with type-(c) behavior.

5. Inflation-deflation behavior due to swelling agent redistribution at a fixed pressure

The findings of the previous Section 4 have immediate and interesting consequences for inflating and deflating a spherical shell simply by altering the distribution of the fixed added mass swelling agent without changing the pressure. For the purposes of this continuing discussion, we continue with the material and structure characterized by (33). In addition, we also now limit attention to $\Delta V/R_i^3 = 3.20$. Together this gives the family of inflation graphs depicted in figures 5 and 6.

Using these figures suppose that the sphere is pressurized with $\Delta P = 0.08\mu$ and that this level of pressurization is maintained as swelling agent is redistributed. This redistribution, which amounts to varying v_i, corresponds to then shifting between the various inflation graphs in figures 5 and 6 at the height determined by $\Delta P/\mu = 0.08\mu$. This will generate changes in r_i/R_i. The least value is $r_i/R_i = 6.78$ which occurs on the inflation graph for $v_i = 1$. The largest value is $r_i/R_i = 10.31$ which occurs on the inflation graph for $v_i = 3.21$. Figure 11 shows r_i/R_i as a function of v_i for $\Delta P = 0.08\mu$.

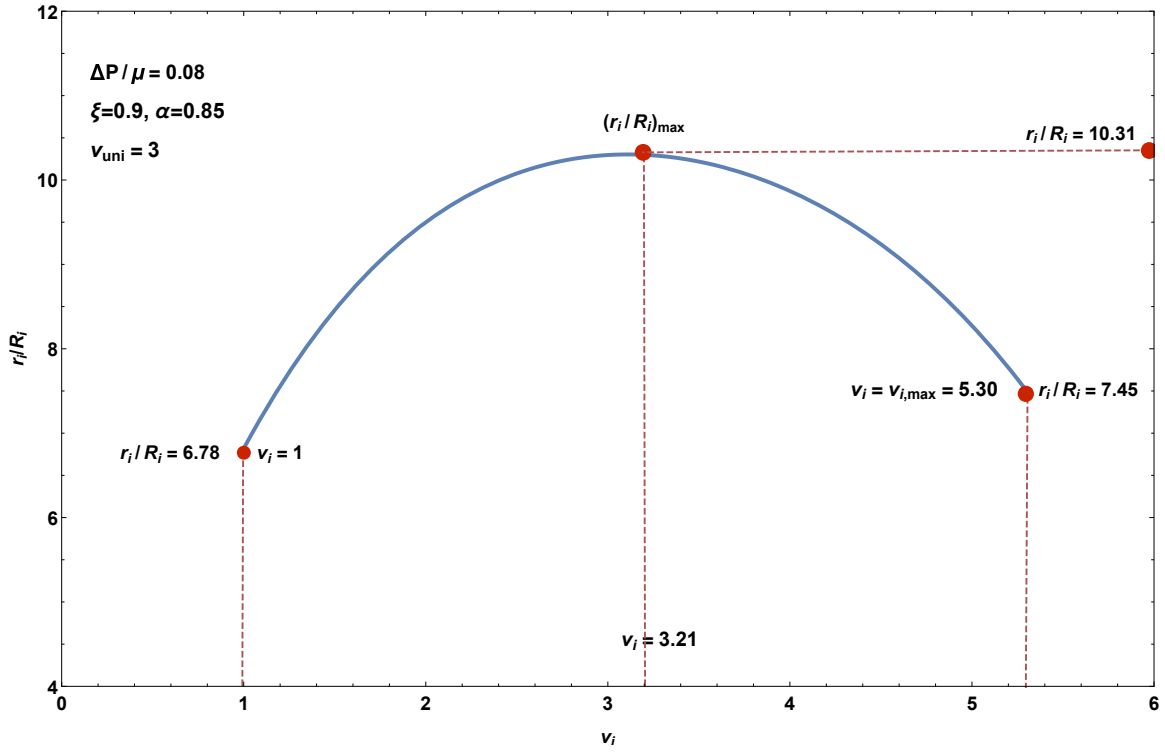

Figure 11. Inflation in terms of r_i/R_i as a function of v_i for (33) with $\Delta V/R_i^3 = 3.20$, which correspond to the sequence of inflation graphs in figures 5 and 6. This specific figure corresponds to $\Delta P = 0.08\mu$. The graph is well behaved, first monotonically increasing (where the correlation is with Figure 5) and then monotonically decreasing (correlated with Figure 6).

The graph in Figure 11 can be generated by moving in figures 5 and 6 along the horizontal line $\Delta P/\mu = 0.08\mu$. Starting at $v_i = 1$ one first moves to the right along this line in Figure 5 whereupon one passes through a sequence of inflation graphs corresponding to continuously increasing v_i until encountering the rightmost inflation graph along that line, which in this case is that for $v_i = 3.21$. This rightmost inflation graph gives the distribution with the maximum inflation for that value of ΔP. All of this generates the first portion of Figure 11 which shows its monotonic increase to $(r_i/R_i)_{\max}$. Note that the just-described construction using Figure 5 passes through all the inflation graphs corresponding to $1 \le v_i \le 3.21$ in a one-to-one fashion. We now come back along the same horizontal line, but now using Figure 6 in order to pass through the remaining inflation graphs, namely those corresponding to $3.21 < v_i \le v_i^{\max}$. This also happens in a one-to-one fashion with increasing v_i during this leftward traversal. Now, because r_i decreases as v_i increases, one generates the rest of Figure 11, namely the part with the monotonic decrease.

As shown by Figure 11 the maximum inflation occurs when $v_i = 3.21$ which is close to the value v_{uni} where the swelling agent is dispersed in a uniform fashion throughout the shell wall. As the swelling agent is increasingly concentrated toward either the inner or outer boundary of the wall, then the radius

decreases. The fact that r_i/R_i in Figure 11 is a single-valued function of v_i is because the height corresponding to $\Delta P = 0.08\mu$ in figures 5 and 6 gives a single encounter with each inflation graph during the right and leftward traversals along the associated horizontal line. Alternatively stated, the type-(c) behavior of the inflation graphs, even with their nonmonotone behavior, has no effect on the process when $\Delta P = 0.08\mu$ because that is well above the graph locations where the nonmonotonicity takes place.

The situation is more complicated if the value of $\Delta P/\mu$ corresponds to a height in either Figure 5 or Figure 6 where the nonmonotonicity of the inflation graphs comes into play. Take $\Delta P/\mu = 0.055$ for which the graph of r_i/R_i versus v_i is shown in Figure 12. To understand why the graph in Figure 12 does not correspond to a single valued function of v_i, note that the value $\Delta P/\mu = 0.055$ now puts one squarely in a region of both Figure 5 and Figure 6 where certain inflation graphs are encountered three times along the horizontal segment: first on an ascending branch, then on its descending branch, and then on the other ascending branch. For the rightward traversal using Figure 5 beginning at $v_i = 1$ this gives rise to the S-shaped graph portion of Figure 12 prior to the maximum inflation at $(r_i/R_i)_{\max}$. As regards the maximum inflation itself, it corresponds to the rightmost inflation graph for $\Delta P/\mu = 0.055$, again this is $v_i = 3.21$. After the maximum in Figure 12, the remaining portion of the graph is generated by the leftward motion along the $\Delta P/\mu = 0.055$ line in Figure 6, meaning that now v_i increases from $v_i = 3.21$ to $v_i^{\max}$. A similar triple intersection phenomena occurs in this leftward traversal, and so there is a corresponding reentrant (doubling-back) portion to Figure 12 after the maximum inflation location.

The two portions of Figure 12 shown in red correspond to points on decreasing portions of the inflation graphs in figures 5 and 6. In the context of a single fixed pressure-inflation graph, increasing graph portions are classically stable. However decreasing graph portions are classically unstable [Ericksen 1975]. To be more precise, a location on an increasing graph portion corresponds to a local energy minimum, whereas a location on a decreasing graph portion corresponds to a local energy maximum. Consequently, from the perspective of energy minimization, should the system ever find itself with an inflation amount corresponding to a location on an unstable branch, the system can lower its energy while maintaining the same pressurization by transitioning to either of the two other equilibrium positions, namely those associated with the two increasing branches. Both of these alternatives are locally stable because they are local minima of energy, although one will involve a lower overall energy (the global minimum). Without belaboring the local versus global minimum distinction, the broader point is that, from a stability perspective, the red portions of Figure 12 will be avoided altogether as the swelling agent is redistributed through the system, i.e., as v_i varies.

Let us consider the consequences by contrasting the two cases of figures 11 and 12 which correspond to the same system at two different pressures. For both pressures we have that $1 \le v_i \le 5.30 = v_i^{\max}$ parameterizes a continuous family of harmonic swelling distributions (23); this means that the same amount of swelling agent is redistributed in a continuous fashion. This in turn leads to changes in the overall inflation, in fact very large changes. For $\Delta P = 0.08\mu$ this inflation change occurs in a continuous fashion as shown in Figure 11. However, for $\Delta P = 0.055\mu$ avoiding the unstable portions of Figure 12 does not allow the same type of continuous inflation. Instead, it is necessary to discontinuously transition (i.e., jump) between the various graph portions of Figure 12. This leads to transition regions as shown in Figure 13. Continuous redistribution of swelling agent corresponding to v_i fully traversing either $1.63 \le v_i \le 1.70$ or $4.79 \le v_i \le 4.89$ are interpreted as requiring jump transitions on Figure 13 that correspond to abrupt change in inflation (without altering $v(R)$, the swelling agent distribution).

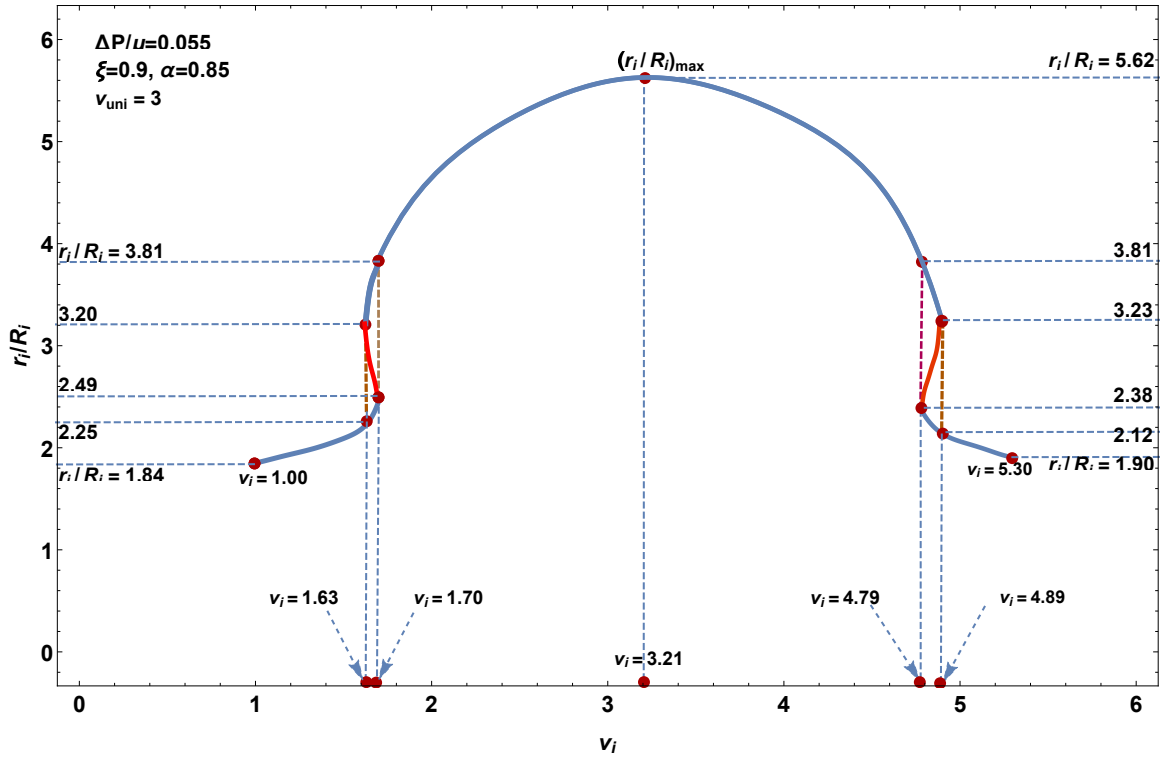

Figure 12. Inflation in terms of r_i/R_i as v_i varies for (33) with $\Delta V/R_i^3 = 3.20$, which again corresponds to the inflation graphs in figures 5 and 6. Here $\Delta P/\mu = 0.055\mu$. In contrast to Figure 11, the graph is not a single valued function of v_i.

The obvious next question that arises is how to determine the jump locations in Figure 13? Ultimately, that is an issue that requires broadening the analysis framework so as to include a specific stability criterion. Any such broadening must address the connection to the underlying physical considerations (e.g., what is the nature of local perturbations that may disrupt equilibrium at a local minimum so as to invoke a transition to the global minimum?). For a case where equilibrium at a local minimum can persist until the local minimum itself vanishes, one obtains a maximum delay type of convention, and this is indicated by the red arrows in Figure 13. Consequently, under such a criterion one obtains a classical hysteresis behavior. On the other hand, there is certainly a particular value in each of the intervals $1.63 \leq v_i \leq 1.70$ and $4.79 \leq v_i \leq 4.89$ where the two local energy values happen to coincide. At that particular value the global minima switches from being on the first stable branch to the second stable branch. Taking that as an alternative stability criterion locates an intermediate value in each of the hysteresis regions in Figure 13 where a common directionally independent transition would occur. The intermediate value on $1.63 \leq v_i \leq 1.70$ would correspond to the particular inflation graph in Figure 5 that causes the horizontal pressure line to correspond to the classical Maxwell line (equal area) construction [Ericksen 1975]. Similarly, the intermediate value on $4.79 \leq v_i \leq 4.89$ would correspond to the particular inflation graph in Figure 6 that also causes the horizontal pressure line to correspond to this same sort of equal area construction.

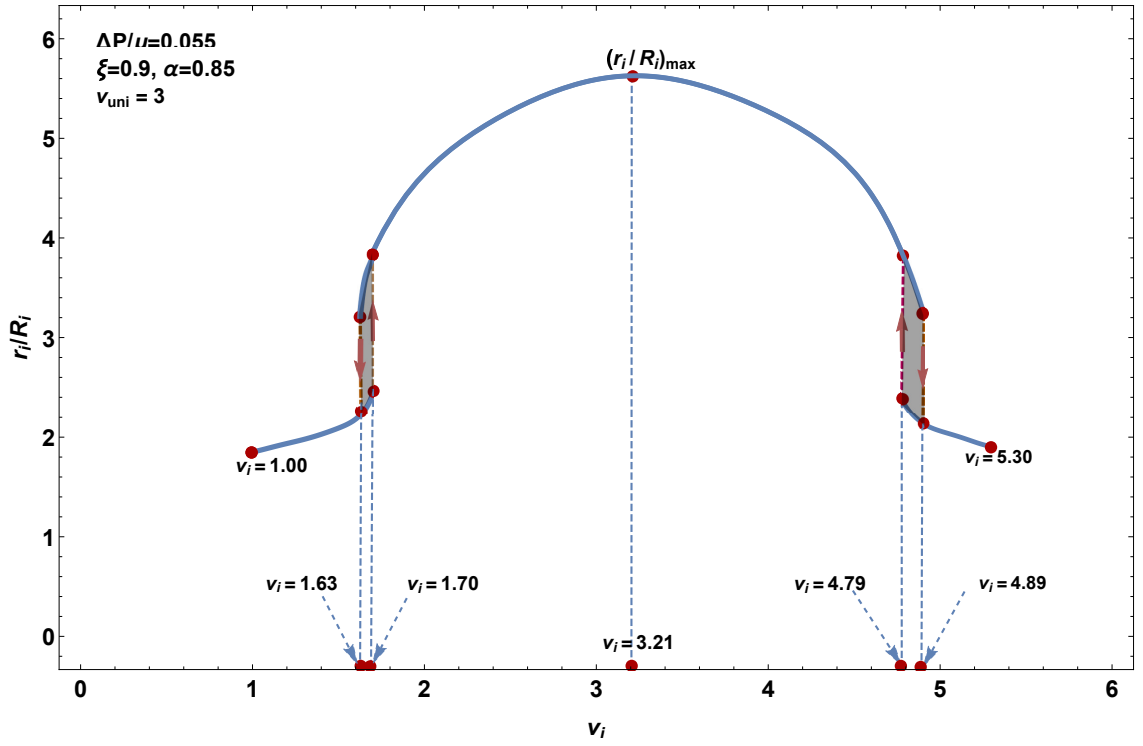

Figure 13. Because the graph in Figure 12 does not establish r_i as a single valued function of v_i, the swelling agent redistribution involves abrupt jumps (limited bursts of inflation). These are restricted to the transition regions as shown. One possibility is the classical hysteresis behavior that involves jumps at the endpoints of the transition regions (red arrows).

For our present purposes we do not wish for these interesting albeit finer stability distinctions to obscure the broader point, which is that the unstable graph portions of Figure 12 give rise to jump-like transitions in inflation as the swelling agent redistributes itself in a completely smooth fashion. For the example corresponding to Figure 12 these jump transitions, or limited inflation bursts, occur in relatively narrow windows of the overall swelling agent redistribution as indicated by the jump regions of Figure 13.

6. Final remarks including study limitations and connection to broader issues

The mechanical properties of porous soft matter are generally dependent upon the amount of liquid that is locally present. As liquid enters (or exits) it causes the material to swell (deswell) and this can lead to unexpected types of deformation. In addition to the local volume change due to the liquid redistribution, there is also the possibly altered structural load response. In this work we have examined these issues in the context of a classical spherical shell.

Specifically, we have considered a spherical shell whose walls are composed of a porous ground substance hyperelastic material that contains a fixed amount of mobile liquid swelling agent. We consider the effect of liquid redistribution in this context, where the redistribution is always radially symmetric.

This preserves the radial symmetry so that the shell is always spherical. Both ground substance and mobile liquid are regarded as individually incompressible. It is presumed that there are no voids in the wall material. Thus the volume of the shell wall is a constant. It is a soft material wall that surrounds the interior spherical region, and the interior spherical region can expand or contract as determined by the shell wall stiffness that provides resistance to any internal pressurization.

Formulating and examining the boundary value problem for modeling this spherical inflation was the object of this paper where the focus was on the combined affect of internal pressure and swelling agent redistribution within the shell wall. Among our findings was that the redistribution of the fixed amount of liquid swelling agent could significantly change the overall expansion. For a fixed pressurization the most expansion was found to occur when the liquid was uniformly distributed throughout the shell wall. Altering the distribution so that the swelling agent was highly concentrated near either the inner or the outer wall surface was found to give less expansion. Thus an active redistribution of liquid within the wall was found to significantly modulate the overall volume.

These findings were obtained in the context of a specific example — meaning a specific choice of structural and material model. The simple spherical geometry essentially rendered the structural model as one described by two degrees of freedom: (1) the wall thickness in the reference state when no free liquid is present and no pressure is applied, and (2) the amount of swelling agent that is then introduced. The first of these degrees of freedom is described by the parameter ξ and the second by the parameter ΔV.

The liquid swelling agent is treated as an incompressible fluid and the ground substance is treated as an incompressible porous hyperelastic material. The resulting state of mixture is described by the field variable v which gives the local volume change from the original ground substance reference state ($v = 1$). Thus v also serves as a direct proxy for the liquid volume fraction. Attention was restricted to equilibrium situations, meaning that any liquid migration has ceased and the liquid has settled into a specific distribution. The resulting equilibrated material was treated as hyperelastic with a stored energy density W that depends on both deformation gradient $\boldsymbol{F}$ (as in conventional hyperelasticity) and the swelling field v. In the absence of additional liquid ($v = 1$) this W was taken to reduce to a conventional Mooney–Rivlin form described in terms of the material parameter α. The extension to include swelling maintained the Mooney–Rivlin model form, while introducing possible swelling sensitivity via q_1 and q_2. The different liquid distributions were described in terms of a simple model expression that we referred to as harmonic. A single variable v_i served to parameterize a complete family of distributions for a fixed amount of swelling agent (described by ΔV). The internal pressure P was the single load parameter. Thus, by virtue of these modeling choices, the resulting problem was described by two structure parameters (ξ, ΔV), three material parameters (α, q_1, q_2), one normalized load parameter P/μ, and one liquid distribution parameter v_i.

Among the limitations of the present work is that only one choice for (α, q_1, q_2, ξ) was examined in any deep way, namely the well motivated values $(\alpha, q_1, q_2, \xi) = (0.85, 0, 0, 0.9)$. As seen from Figure 2, the corresponding (α, ξ) point is in the type-(c) region for behavior in the absence of swelling ($\Delta V = 0$) which also makes it the behavior for any $\Delta V > 0$ so long as the liquid swelling agent is uniformly distributed. Importantly, the point $(\alpha, \xi) = (0.85, 0.9)$ in Figure 2 is near the boundary of the type-(c) to type-(a) transition for uniform swelling distributions.

Along with $q_1 = q_2 = 0$ the focus on $(\alpha, \xi) = (0.85, 0.9)$ allowed us to consider the detailed affect of the remaining three parameters ΔV, v_i and P/μ. In this context a rich variety of behaviors was observed.

Some attempt to codify our behavior findings led to the diagram displayed in Figure 4 which may be viewed as a type of *liquid redistribution structural response map* for the particular pair (α, ξ) that was the focus of our developed example.

Among the issues not treated in the present work are how the response might alter for the consideration of other (α, ξ) pairs. In other words, viewing Figure 2 as a sort of *global phase diagram*, each point of that phase diagram would itself generate a liquid redistribution structural response map akin to that displayed in Figure 4. The possible variation in these response maps would seem to be of some interest. The question arises as to the effect of alternative constitutive models beyond that of the relatively well known Mooney–Rivlin form that is the focus of this paper. Even more general issues concern any possible compressibility in the individual constituents as well as the consideration of alternative deformation modes not connected to spherical symmetry. For this purpose, [Tsai et al. 2004] is of some possible relevance in view of its discussion on the contrasting roles of compressibility versus incompressibility in a case of swelling induced bending for a boundary value problem that can be viewed in terms of a cantilevered beam.

Finally, the issue of the physics behind the liquid agent redistribution was not treated. In particular, v_i was regarded as a control variable that was at our disposal. One might consider either passive or active mechanisms for achieving such control and thus redistributing the fixed amount of liquid. Their detailed consideration would most likely encounter important questions related to the broader thermodynamics of the envisaged process. In this regard, the present study has chosen to focus on the specific modeling issues associated solely with the mechanics of materials and structures portion of any such broader analysis.

Acknowledgment

This work is made possible by NPRP grant nos. 4-1333-1-214 and 8-2424-1-477 from the Qatar National Research Fund (a member of Qatar Foundation). The statements made herein are solely the responsibility of the authors.

References

[Amar and Ciarletta 2010] M. B. Amar and P. Ciarletta, "Swelling instability of surface-attached gels as a model of soft tissue growth under geometric constraints", *J. Mech. Phys. Solids* **58**:7 (2010), 935–954.

[Bowen 1980] R. M. Bowen, "Incormpressible porous medium models by the use of the theory of mixtures", *Int. J. Eng. Sci.* **18** (1980), 1129–1148.

[Carroll 1987] M. M. Carroll, "Pressure maximum behavior in inflation of incompressible elastic hollow spheres and cylinders", *Quart. Appl. Math.* **XLV**:1 (1987), 141–154.

[Cheng et al. 2019] J. Cheng, Z. Jia, H. Guo, Z. Nie, and T. Li, "Delayed burst of a gel balloon", *J. Mech. Phys. Solids* **124** (2019), 143–158.

[Chester and Anand 2010] S. A. Chester and L. Anand, "A coupled theory of fluid permeation and large deformations for elastomeric materials", *J. Mech. Phys. Solids* **58**:11 (2010), 1879–1906.

[Drozdov 2013] A. D. Drozdov, "Finite elasticity of nanocomposite hydrogels", *Compos. Interfaces* **20**:9 (2013), 673–692.

[Drozdov et al. 2018] A. D. Drozdov, J. Christiansen, and J. deClaville, "Time-dependent response of hydrogels under multi-axial deformation accompanied by swelling", *Acta Mech.* **229** (2018), 5067–5092.

[Duda et al. 2010] F. P. Duda, A. C. Souza, and E. Fried, "A theory for species migration in a finitely strained solid with application to polymer network swelling", *J. Mech. Phys. Solids* **58**:4 (2010), 515–529.

[Duda et al. 2011] F. P. Duda, A. C. Souza, and E. Fried, "Solvent uptake and cavitation", *J. Mech. Phys. Solids* **59**:11 (2011), 2341–2354.

[Ericksen 1975] J. L. Ericksen, "Equilibrium of bars", *J. Elasticity* **5**:3 (1975), 191–201.

[Fang et al. 2008] Y. Fang, T. J. Pence, and X. Tan, "Nonlinear elastic modeling of differential expansion in trilayer conjugated polymer actuators", *Smart Mater. Struct.* **17**:6 (2008), 065020.

[Goriely et al. 2010] A. Goriely, D. E. Moulton, and R. Vandiver, "Elastic cavitation, tube hollowing, and differential growth in plants and biological tissues", *EPL* **91**:1 (2010), 18001.

[Gou and Pence 2016] K. Gou and T. J. Pence, "Hyperelastic modeling of swelling in fibrous soft tissue with application to tracheal angioedema", *J. Math. Biol.* **72** (2016), 499–526.

[Green and Shield 1950] A. E. Green and R. T. Shield, "Finite elastic deformation of incompressible isotropic bodies", *Proc. R. Soc. A* **202**:1070 (1950), 407–419.

[Liu et al. 2018] S. L. Z. Liu, E. Boatti, K. Bertoldi, and R. Kramer-Bottiglio, "Stimuli-induced bi-directional hydrogel unimorph actuators", *Extreme Mech. Lett.* **21** (2018), 35–43.

[Mihai et al. 2019] L. A. Mihai, D. Fitt, T. E. Woolley, and A. Goriely, "Likely equilibria of stochastic hyperelastic spherical shells and tubes", *Math. Mech. Solids* **24**:7 (2019), 2066–2082.

[Müller and Strehlow 2004] I. Müller and P. Strehlow, *Rubber and rubber balloons: paradigms of thermodynamics*, vol. 637, Springer, 2004.

[Pence 2012] T. J. Pence, "On the formulation of boundary value problems with the incompressible constituents constraint in finite deformation poroelasticity", *Math. Methods Appl. Sci.* **35** (2012), 1756–1783.

[Pence and Tsai 2006] T. J. Pence and H. Tsai, "Swelling-induced cavitation of elastic spheres", *Math. Mech. Solids* **11**:5 (2006), 527–551.

[Selvadurai and Suvorov 2018] A. P. S. Selvadurai and A. P. Suvorov, "On the development of instabilities in an annulus and a shell composed of a poro-hyperelastic material", *Proc. R. Soc. A* **474**:2218 (2018), 20180239.

[van der Sman 2015] R. G. M. van der Sman, "Hyperelastic models for hydration of cellular tissue", *Soft Matter* **11**:38 (2015), 7579–7591.

[Stuart et al. 2010] M. A. C. Stuart, W. T. S. Huck, J. Genzer, M. Müller, C. Ober, M. Stamm, G. B. Sukhorukov, I. Szleifer, V. V. Tsukruk, M. Urban, et al., "Emerging applications of stimuli-responsive polymer materials", *Nat. Mater.* **9**:2 (2010), 101–113.

[Treloar 1975] L. R. G. Treloar, *The physics of rubber elasticity*, Oxford University Press, 1975.

[Truesdell 1962] C. Truesdell, "Mechanical basis of diffusion", *J. Chem. Phys.* **37** (1962), 2336–2334.

[Tsai et al. 2004] H. Tsai, T. J. Pence, and E. Kirkinis, "Swelling induced finite strain flexure in a rectangular block of an isotropic elastic material", *J. Elasticity* **75**:1 (2004), 69–89.

[Yavari and Goriely 2013] A. Yavari and A. Goriely, "Nonlinear elastic inclusions in isotropic solids", *Proc. R. Soc. A* **469**:2160 (2013), 20130415.

[Zamani and Pence 2017] V. Zamani and T. J. Pence, "Swelling, inflation, and a swelling-burst instability in hyperelastic spherical shells", *Int. J. Solids Struct.* **125** (2017), 134–149.

Received 20 Aug 2019. Revised 31 Dec 2019. Accepted 10 Jan 2020.

VAHID ZAMANI: zamaniva@msu.edu
Department of Mechanical Engineering, Michigan State University, Engieering Building, East Lansing, MI 48824-1226, United States

THOMAS J. PENCE: pence@egr.msu.edu
Department of Mechanical Engineering, Michigan State University, Engineering Building, East Lansing, MI 48824-1226, United States

JOURNAL OF MECHANICS OF MATERIALS AND STRUCTURES

msp.org/jomms

Founded by Charles R. Steele and Marie-Louise Steele

Cover photo: Ev Shafrir

See msp.org/jomms for submission guidelines.

JoMMS (ISSN 1559-3959) at Mathematical Sciences Publishers, 798 Evans Hall #6840, c/o University of California, Berkeley, CA 94720-3840, is published in 10 issues a year. The subscription price for 2020 is US $660/year for the electronic version, and $830/year (+$60, if shipping outside the US) for print and electronic. Subscriptions, requests for back issues, and changes of address should be sent to MSP.

JoMMS peer-review and production is managed by EditFLOW® from Mathematical Sciences Publishers.

PUBLISHED BY

mathematical sciences publishers

nonprofit scientific publishing

http://msp.org/

Journal of Mechanics of Materials and Structures

Volume 15, No. 1 January 2020

1559-3959(2020)15:1;1-L